ELSEVIER

Beating hydrogen with its own weapon: Nano-twin gradients enhance embrittlement resistance of a high-entropy alloy

Hong Luo, Wenjun Lu, Xufei Fang, Dirk Ponge, Zhiming Li *, Dierk Raabe *

Max-Planck-Institut für Eisenforschung, Max-Planck-Straße 1, 40237 Düsseldorf, Germany

High-entropy alloys have shown exceptional damage tolerance at cryogenic temperatures. Here we report that this essential property can be maintained even when exposing the equiatomic CoCrFeMnNi alloy to the most detrimental environmental condition known to metals, hydrogen. This is enabled by a self-accommodation mechanism: the higher the local hydrogen content, the higher the twin formation rate as hydrogen reduces the stacking fault energy. Thus, the hydrogen's through thickness diffusion gradient translates into a nano-twin gradient that counteracts material weakening by enhanced local strengthening. The concept targets applications under harsh and cryogenic conditions, such as encountered in arctic, offshore, energy and liquid gas chemical processing, and transport operations. The new mechanism opens a pathway to the design of alloys that withstand heavy mechanical loading under cryogenic and hydrogen-containing conditions.

Introduction

High-entropy alloys (HEAs) composed of multiple principal elements have drawn great attention over the past decade [1–6]. The five-component equiatomic CoCrFeMnNi alloy is one of the most appealing HEAs due to the high thermodynamic stability of its single face-centered cubic (f.c.c.) structure and the excellent mechanical properties at various temperatures [7]. It also shows good resistance to hydrogen embrittlement at relatively low hydrogen concentrations [8,9]. However, it suffers from embrittlement at high hydrogen concentrations during slow strain rate tensile deformation [10,11]. Hydrogen has long been known to cause embrittlement, which is a severe environmental type of failure that affects almost all metals and alloys. In non-hydride forming materials, e.g., the aforementioned CoCrFeMnNi HEA, the deleterious effects of hydrogen on the mechanical properties are mainly due to the element's influence on dislocation multiplication, glide, and patterning, as well as on interface decohesion [12].

Although the threat of hydrogen embrittlement has motivated nearly one and a half centuries of intense research [13–21], hydrogen remains not only the most ubiquitous but also the least understood element in engineering metallic alloys. Further, the applied temperature has remarkable effects on the mechanical properties of materials in the presence of hydrogen [22,23]. For instance, metastable stainless steels are susceptible to hydrogen embrittlement particularly between 200 and 300 K [24,25]. At liquid nitrogen temperature (77 K), hydrogen embrittlement is generally less studied in metallic materials [26]. Specifically in HEAs, the effects of hydrogen under cryogenic conditions are still unclear.

Here, we show how the addition of hydrogen fundamentally changes the deformation behavior of an equiatomic CoCrFeMnNi HEA at 77 K due to the formation of a nano-twin gradient structure extending over 35 μm from the surface with nanoscale twins to the sample center with coarse twins. This gradient in the nano-twin population provides additional local strain hardening reserves, suppressing the material's surface embrittlement.

Twin-gradient-related strategies for improving the mechanical properties of metals were reported before in the example of copper, which was subjected to surface mechanical grinding for achieving gradient nano-structures [27,28]. Here we use chemical

* Corresponding authors.
E-mail addresses: Li, Z. (zhiming.li@mpie.de), Raabe, D. (d.raabe@mpie.de).

 https://doi.org/10.1016/j.mattod.2018.07.015

instead of mechanical grading for creating such nanostructure profiles. The key mechanism behind this phenomenon in the current HEA lies in the influence of the local hydrogen concentration on the phase stability of the f.c.c. lattice structure: In the surface region, where the hydrogen content is high, the HEA's phase stability is reduced rendering it prone to intense nano-twin formation upon cryogenic loading. In the mid-thickness sample region, less hydrogen was accumulated, hence leaving the material's properties widely unaltered.

The equiatomic CoCrFeMnNi HEA was produced by melting and casting in a vacuum induction furnace from high-purity metals. The cast alloy was hot-rolled and homogenized followed by water-quenching. Grain size was refined by cold-rolling and recrystallization annealing. Uniaxial tensile specimens of ASTM standard G129 were cut by wire-electrode discharge machining.

Results and discussion

Fig. 1a shows the tensile curves of CoCrFeMnNi HEA samples tested at 77 K with and without hydrogen charging. The yield strength and ultimate tensile strength of the samples at 77 K devoid of hydrogen are about 430 MPa and 950 MPa (Supplementary Table 1), respectively, showing significantly increased values compared to those at room temperature [9]. Most importantly though, the HEA sample tested at 77 K did not show any significant degradation in strength and ductility when exposed to hydrogen charging (Fig. 1a). This indicates that the CoCrFeMnNi HEA has excellent resistance to hydrogen embrittlement at liquid nitrogen temperature. The thermal desorption spectroscopy (TDS) analysis results shown in Fig. 1b confirms that the total concentration of hydrogen is ~53.6 wt.ppm after electrochemical charging prior to tensile testing.

To understand the micromechanisms during cryo-deformation of the hydrogen-charged HEA, we analyzed the microstructures of the cross-section in the tensile-tested sample ~200 μm away from the fracture surface, covering a range from the surface to the inner regions following the decreasing hydrogen concentration. Fig. 2a and b present EBSD maps of the HEA sample after tensile testing at 77 K without hydrogen charging. The grains are elongated along the loading direction and some deformation twins are observed in the grain interior (Fig. 2b). This observation matches previous studies showing that twinning is indeed an important mechanism during the late deformation stages of the equiatomic CoCrFeMnNi HEA at cryogenic temperature [29,30]. Fig. 2c shows that the line fraction of the deformation twin interfaces relative to all grain boundaries is quite similar in the surface and the interior regions for the uncharged specimen.

In contrast, the HEA sample tested at 77 K after hydrogen charging shows two significant differences to the hydrogen free sample: First, it contains a much higher density of deformation twin boundaries (Fig. 2e and f) than its hydrogen-free counterpart. Second, the density of the twin boundaries and their line fraction are much higher in the hydrogen-rich surface region than in the hydrogen poor inner region (Fig. 2g), establishing a nano-twin gradient structure after cryo-deformation. Such a nano-twinned gradient structure enabled by chemical gradients is observed for the first time in the present study.

To identify also corresponding structure – property features relating the twin-structure to the mechanical response, nanoindentation tests were conducted on the cross section of the tensile-tested HEA samples for both, hydrogen charged and uncharged samples. Prior to indentation samples were heated to 373 K for 3 days and kept at 273 K for 7 days to ensure removal of all hydrogen so as to probe the effect of the nanostructure gradient only. Fig. 2d shows the nanohardness of the regions in the cross section ~200 μm away from the fracture surface. The nanohardness data of the HEA sample that was free of any hydrogen when cryo-tensile tested, i.e., without gradient nano-twin structure, show similar hardness values in the inner and outer portions of the sample.

In contrast, the sample that was hydrogen charged prior to cryo-tensile testing reveals a nanohardness gradient that matches the nano-twin structure gradient (Fig. 2h). This means that the sample shows higher nanohardness values in the outer region

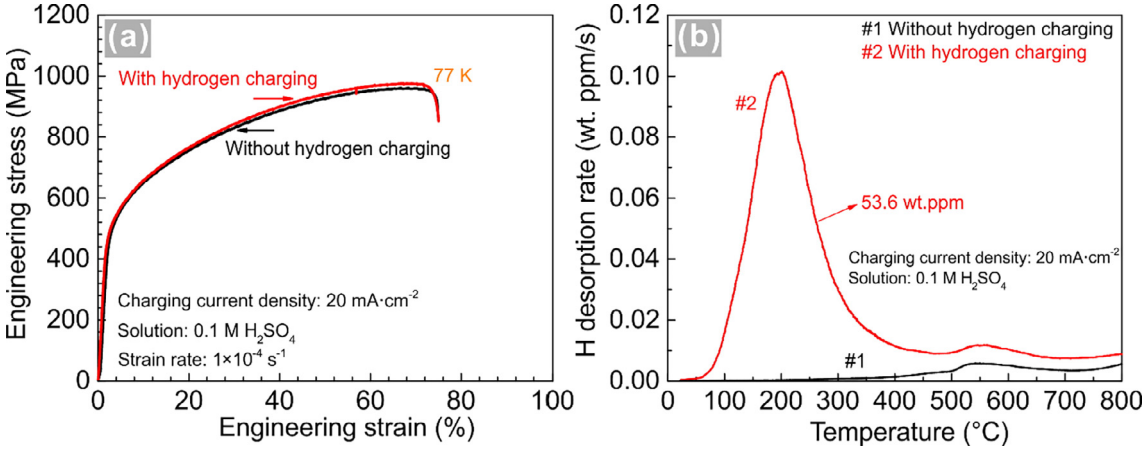

FIGURE 1

Mechanical behavior of equiatomic CoCrFeMnNi HEA upon deformation at 77 K with and without hydrogen. (a) Tensile stress–strain curves with and without hydrogen exposure. (b) Hydrogen desorption rate curves of the samples prior to deformation. The total hydrogen concentration was 53.6 wt.ppm after hydrogen charging.

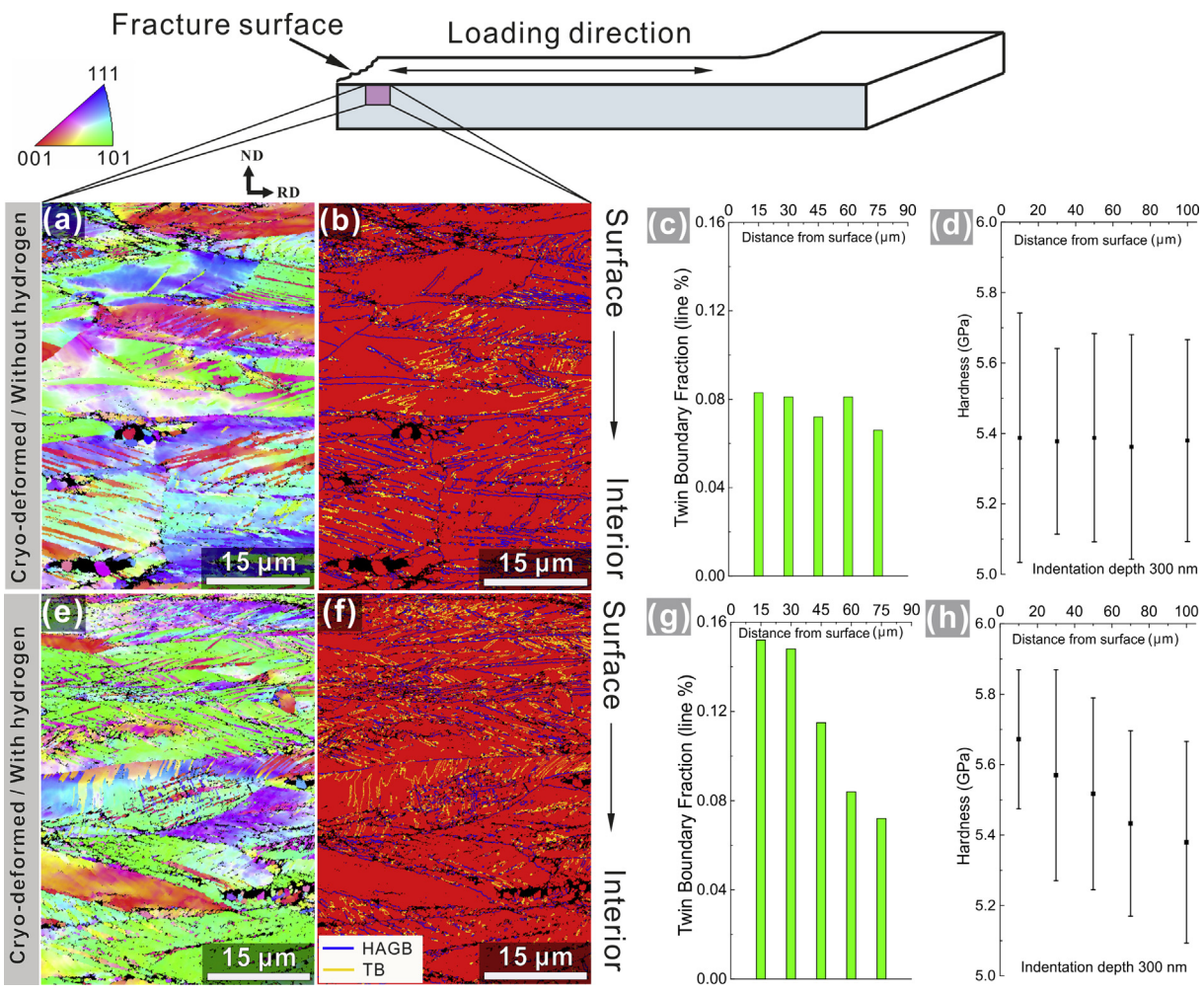

FIGURE 2

Microstructures in the equiatomic CoCrFeMnNi HEA samples after cryo-deformation. (a,b) IPF and grain boundary maps of the cryo-deformed sample without hydrogen showing few deformation-induced twins. (c) Line fraction of deformation twins from the surface to the interior. (d) Cross sectional nanohardness in the cryo-tensile-tested sample without prior hydrogen charging, i.e., without gradient nano-twin structure. (e,f) IPF and grain boundary maps of the cryo-deformed sample with hydrogen showing a very high density of deformation twins, especially in the region near to the surface of the sample. (g) Line fraction of deformation twins from the surface to the interior revealing a gradient nano-twin structure. (h) Cross sectional nanohardness in the cryo-tensile-tested sample with prior hydrogen charging, i.e., with gradient nano-twin structure. The nanoindentation experiments were conducted on the cross section of the cryo-tensile-tested HEA samples after hydrogen was removed by heating. IPF: inverse pole figure. HAGB and TB refer to high-angle grain boundary and twin boundary, respectively. Twin boundaries' line fractions refer to the percentage of the length of deformation twin boundaries relative to the total high-angle grain boundary length.

where the nano-twin density was higher than in the inner region where it was lower. Since the hydrogen itself was removed from the sample prior to indentation this observation reveals that the high density of the nano-twins creates a local hardening effect, consistent to previous work showing that the local hardness scales with the nanoscale twin content in f.c.c. metals [31].

We further revealed the nano-twinned gradient structure by transmission electron microscopy (TEM). TEM specimens were taken by site-specific lift-out using a FIB and prior EBSD measurements to select regions of interest (Fig. 3a). The TEM images of the specimen from the surface region show a very high density of lamella-shaped features with an average thickness of ~25 nm (Fig. 3b and c). The selected area diffraction (SAD) pattern and the corresponding stereographic projection of the orientation in Fig. 3d confirm that the very fine lamellae are nano-twins. The TEM results of the specimen taken from the inner regions of the deformed sample show much coarser twins with an average twin thickness of ~100 nm (Fig. 3e–g). The TEM results thus reveal a nano-twinned gradient structure with smaller nano-twins with high line density in the surface region and coarser twins with lower line density in the material's inner region. It was reported before that mechanical twinning is an important deformation mechanism in the CoCrFeMnNi HEA, particularly when deformed at 77 K and/or at high deformation rates [29,30]. This earlier finding is confirmed by our results (Fig. 2). Hydrogen is reducing the stacking fault energy, hence promoting this mechanism further. However, without the diffusion controlled near-surface composition gradient of the hydrogen through the material thickness, the resulting enhanced twin density and size distribution would be uniform throughout the bulk sample and hence no gradient-twin structure would be formed.

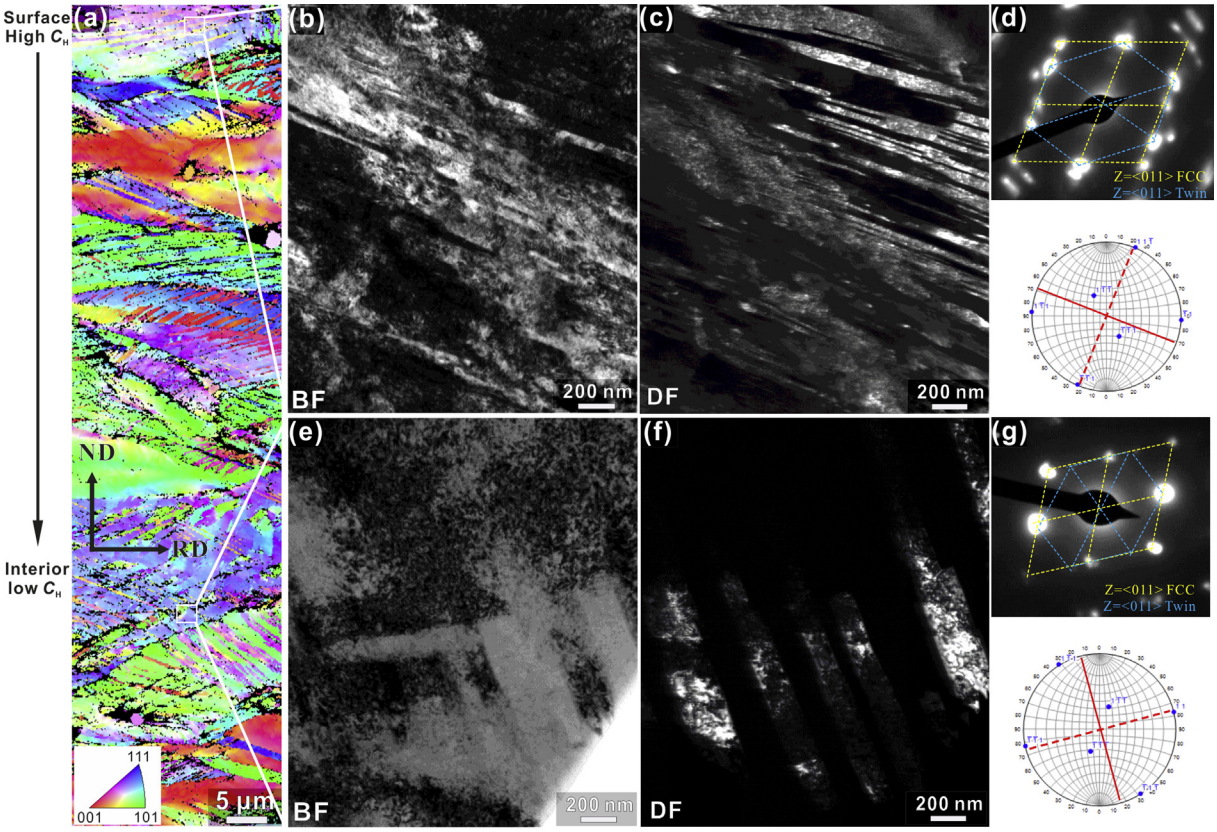

FIGURE 3

Deformation micromechanisms in different regions of the HEA at 77 K. (a) EBSD map showing the cross-section regions selected for further TEM analysis after hydrogen charging and cryo-deformation. (b–d) Bright-field TEM, dark-field TEM, and selected area diffraction (SAD) pattern for a typical surface region. (e–g) Bright-field TEM, dark-field TEM, and SAD pattern for a typical inner region. C_H refers to the concentration of hydrogen.

The fracture morphology corresponding to the gradient nano-twin structure was examined and the results are shown in Fig. 4. There are no features of brittle fracture in the surface regions of samples with and without hydrogen (Fig. 4a and b), proving that the HEA can resist surface brittle fracture in the presence of hydrogen at liquid nitrogen temperature. The fracture surface of the tested sample without preceding hydrogen charging shows the growth and coalescence of microvoids as prevalent failure mechanism (Fig. 4c). The dimple patterns are similar in both the surface and center regions of the tensile sample. The average size of the uniformly distributed dimples is ~1 μm. Inclusion particles are observed in some of the dimples (Fig. 4c). The dimple sizes are not uniform in the hydrogen-charged cryo-tensile-tested HEA samples, and they show a gradual increase from the surface to the center regions (Fig. 4f–h). Specifically, the surface region with its higher hydrogen concentration shows nano-sized dimples with an average size of only ~80 nm (Fig. 4g), while the hydrogen-poor center region has much coarser dimples with an average size of ~1 μm. This gradient in dimple sizes is strongly correlated with the gradient nano-twin structure induced by the hydrogen under cryo-deformation conditions. This means that the finer twins in the surface region also lead to a higher dimple dispersion and, vice versa, coarser twins create larger dimples [32].

Another important feature is that no cracks were observed in the surface region with its high hydrogen concentrations after cryo-tensile deformation (Fig. 4). Numerous previous works [33–37] revealed that surface cracks are readily formed after electrochemical charging and tensile deformation at slow strain rates at room temperature. In general, hydrogen induced cracking is controlled by diffusion of hydrogen and its accumulation at crack tips [38] where hydrogen transport can be enhanced by dislocations. The diffusion of hydrogen decreases exponentially with decreasing temperature. Based on the parameters of hydrogen diffusion in other f.c.c. alloys [39], e.g., the lattice activation energy, the diffusion pre-exponential factor, and the temperature, the lattice diffusion coefficient of hydrogen in the equiatomic CoCrFeMnNi HEA at 77 K was estimated to be in the range of 10^{-35}–10^{-40} $m^2 \cdot s^{-1}$. Another important factor is that the twin boundaries, especially the coherent ones, have been suggested to be inherently resistant to hydrogen embrittlement because of their high surface separation energy, high coherency, and low hydrogen solubility [40,41]. Accordingly, an increased population of twin boundaries induces a nanoscale toughening mechanism, i.e., the cracks can be arrested by twin boundaries, and nanoscale twins serve as crack-bridging ligaments. Atomistic simulations have shown that a large number of necklace-like dislocations can be emitted from a crack tip and interact with twin boundaries ahead of the crack tip, transforming coherent twin boundaries into impenetrable dislocation walls, which can strongly resist crack propagation, leading to crack arresting and bridging [42–44]. Therefore, the gradient nano-twinned structure

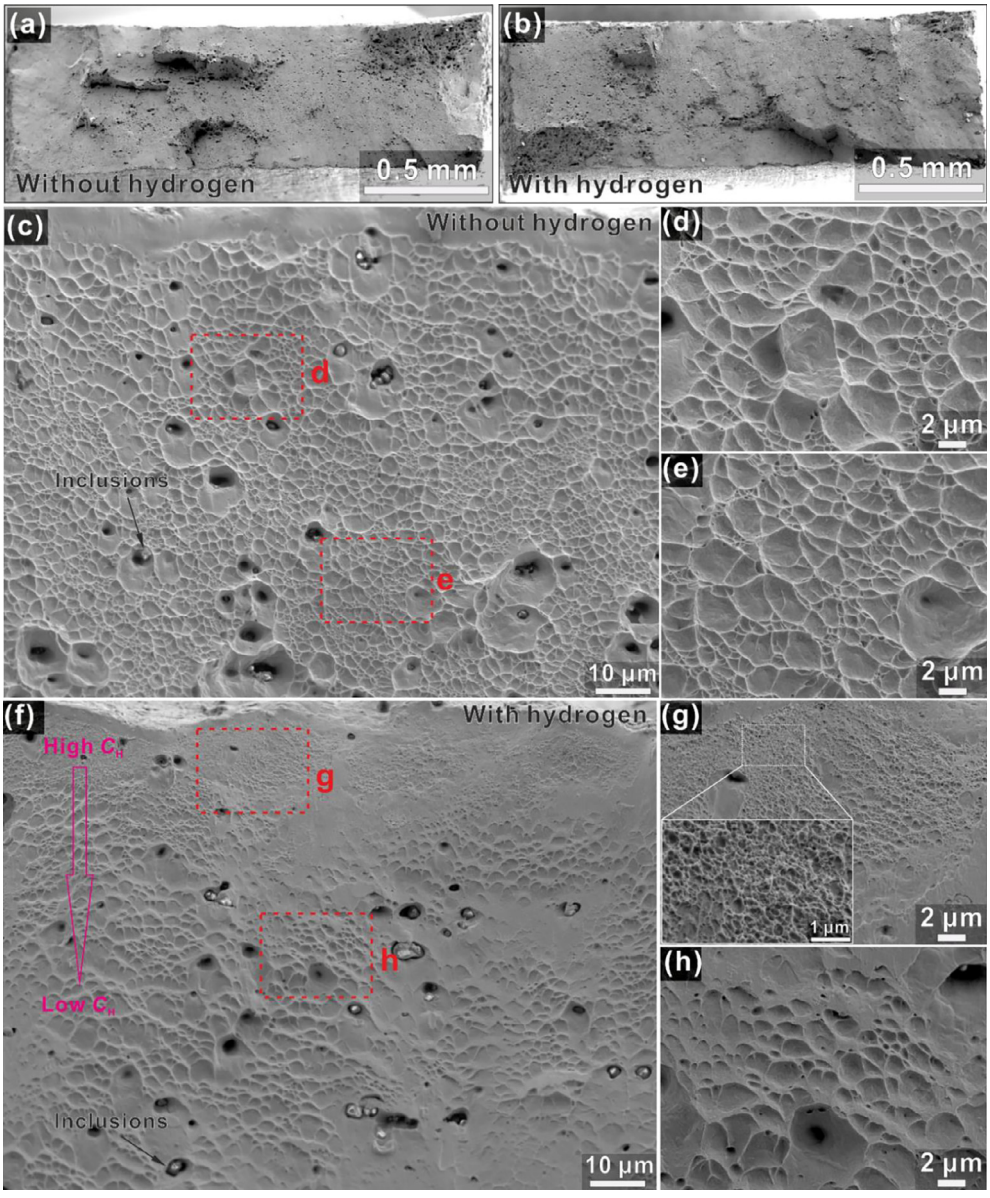

FIGURE 4

Fracture morphologies of CoCrFeMnNi HEA samples after cryo-deformation with and without hydrogen at 77 K. (a,b) Fracture morphologies of HEA samples after tensile testing with and without hydrogen charging. (c) Ductile-dimpled fracture surface of sample without hydrogen charging. (d,e) Enlarged images for edge and center regions of the fracture surface marked in a, respectively. (f) Ductile-dimpled fracture surface of sample with hydrogen charging. (g,h) Enlarged images for edge and center regions of the fracture surface marked in d, respectively. C_H refers to the concentration of hydrogen.

is likely to improve the resistance to surface cracks due to the very high density of nano-twin in the surface region.

These results show that one of the main features of the microstructural evolution in the CoCrFeMnNi HEA upon deformation at 77 K is the intense mechanical twinning. This is consistent with previous work on the cryo-deformation behavior of the CoCrFeMnNi HEA [29] and associated with the low stackingfault energy (SFE) of the HEA, especially when decreasing the deformation temperature [45]. Hydrogen reduces the SFE of f.c.c. materials even further, hence, supporting the earlier onset of mechanical twinning under load. The hydrogen-induced decrease in the stacking fault energy in f.c.c. alloys could be explained by the formation of H-H pairs in the faulted zone, i.e., the recombination of hydrogen atoms occupying neighboring interstitial lattice sites [46,47]. Therefore, the synergistic effects of hydrogen and cryo-deformation lead to a high density of nano-twins in the HEA. As revealed by the fracture surface analysis, hydrogen promotes the formation of more extensive twinning without introducing any embrittlement during cryo-deformation. Since hydrogenation was performed by cathodic charging in the solution, a gradient in hydrogen concentration from the surface to the inner regions of the samples was introduced where the hydrogen concentration in the surface region is much higher than that in the inner regions [48–50]. Therefore, the surface region with its higher hydrogen concentration produces a higher density of nano-twins, while the inner region with its lower hydrogen concentration forms fewer twins and larger twin sizes.

The gradient nano-twin structure in the hydrogen charged sample is expected to also provide a strengthening effect during the later stages of deformation. The strengthening provided by nano-twins is generally attributed to the dynamic Hall–Petch effect, i.e., to the reduction in the mean-free dislocation path [51]. Dislocations accumulated along the twin boundaries are expected to promote a more uniform plastic deformation, enhancing ductility. The high density of partial dislocations and their interactions together with the small average twin spacing both enhance strain hardening. This stabilizes plastic deformation against necking, hence also increasing tensile ductility [52]. However, hydrogen presence during cryo-deformation may also promote certain embrittlement effects for instance due to local hydrogen accumulation as a consequence of its high fugacity in the sample surface region after electrochemical charging in sulfuric acid solution. This means that the strain hardening provided by the gradient nano-twin structure seems to overcompensate hydrogen-induced embrittlement effects (e.g., localized plasticity and void formation) in the CoCrFeMnNi alloy at 77 K. These two opposing effects are mutually compensating at comparable levels so that the gradient nano-twin structure has only a negligible effect on the overall macroscopic flow stress of the CoCrFeMnNi alloy in the current study.

Conclusions

In summary, we showed that a gradient nano-twin structure, characterized by small nano-twins with high line density in the surface region and coarser twins with lower line density in the inner sample regions, can be induced by cryo-tensile deformation in a gradient-hydrogen-charged CoCrFeMnNi HEA. The beneficial effect of the gradient nano-twin structure overcompensates hydrogen embrittlement effects, thus leading to the absence of hydrogen-induced surface cracks upon tensile deformation at 77 K. These observations allow to take a novel approach to the introduction of gradient nanostructures into metallic alloys not through mechanical but through chemical gradients. Realizing this with hydrogen represents a new strategy of designing hydrogen tolerant materials for cryogenic applications by turning it from a harmful to a beneficial element through utilizing its effect on the stacking fault energy.

Materials and methods

Materials preparation

The equiatomic CoCrFeMnNi HEA ingot with dimensions of $25 \times 60 \times 65\ mm^3$ was cast in a vacuum induction furnace using pure metals with predetermined compositions ($Co_{20}Cr_{20}Fe_{20}Mn_{20}Ni_{20}$, at.%). Samples with dimensions of $10 \times 25 \times 60\ mm^3$ machined from the original cast were subsequently hot-rolled at 900 °C to a thickness reduction of 50% (thickness changed from 10 to 5 mm). Homogenization was conducted at 1200 °C for 2 h in Ar atmosphere followed by water-quenching. To refine the grain size, samples were further cold-rolled to a thickness reduction of 60%, and subsequently annealed at a furnace temperature of 900 °C for 3 min in Ar atmosphere followed by water-quenching.

Microstructural and elemental characterization

The microstructure of the recrystallized alloy (grain-refined) was analyzed using various methods. Electron backscatter diffraction (EBSD) measurements were carried out by a Zeiss-Crossbeam XB 1540 FIB scanning electron microscope (SEM) with a Hikari camera and the TSL OIM data collection software. The EBSD analyses were conducted with a beam step size of 5 nm. The fracture morphology was observed by a Zeiss-Merlin instrument. A Phillips CM20 TEM operating at 200-kV accelerating voltage was used to characterize TEM foils by dark-field imaging and selected area diffraction. The TEM foils were prepared by a focus ion beam (FIB) lift-out procedure with final milling at 5 kV.

Hydrogen charging and mechanical characterization

Hydrogen was introduced into the specimens by electrochemical charging with current density 20 mA/cm^{-2} at ambient temperature (25 °C) in 0.1 M H_2SO_4 solution plus 2 $g{\cdot}L^{-1}$ CH_4N_2S. A platinum wire was used as the counter electrode. The samples were pre-charged for 240 h at 20 $mA{\cdot}cm^{-2}$. Then, they were moved to liquid nitrogen environment immediately for tensile tests. The tensile tests were conducted in a Zwick tensile machine at the tensile rate of $1 \times 10^{-4}\ s^{-1}$. Uniaxial tensile tests were conducted using specimens with thickness of 1.0 mm and gauge length of 10 mm. Three samples for each condition were tested to confirm reproducibility. The hydrogen desorption rates were measured using a custom-designed UHV-based Thermal Desorption Analysis instrument in conjunction with a Mass Spectrometer detector set up (TDA-MS) from 25 °C to 800 °C, and the corresponding heating rate was 26 $°C{\cdot}min^{-1}$. The total hydrogen concentration was determined by measuring cumulative desorbed hydrogen from 25 °C to 800 °C. Nanoindentation tests were carried out using a Berkovich diamond tip with the continuous stiffness measurement (CSM) mode on Agilent G200 nanoindenter.

Acknowledgments

This work was financially supported by the European Research Council under the EU's 7th Framework Programme (FP7/2007-2013)/ERC Grant agreement 290998. The author (H.L.) is also supported by the Alexander von Humboldt-Stiftung (www.humboldtfoundation.de).

Data availability

The raw/processed data required to reproduce these findings cannot be shared at this time as the data also form part of an ongoing study.

Author contributions

H.L., Z.L. and D.R. designed the research project; H.L. and W.L. characterized the alloys; H.L. X.F. and Z.L. analyzed the data; H.L., Z.L, D. P. and D. R. wrote the paper.

Appendix A. Supplementary data

Supplementary data associated with this article can be found, in the online version, at https://doi.org/10.1016/j.mattod.2018.07.015.

References

[1] J.W. Yeh et al., Adv. Eng. Mater. 6 (2004) 299–303.
[2] Y. Zhang et al., Prog. Mater Sci. 61 (2014) 1–93.
[3] B. Cantor et al., Mater. Sci. Eng., A 375 (2004) 213–218.
[4] Z. Li et al., Nature 534 (2016) 227–230.
[5] F. Zhang et al., Nat. Commun. 8 (2017) 15687.
[6] R.X. Li et al., Mater. Sci. Eng., A 707 (2017) 668–673.
[7] F. Otto et al., Acta Mater. 61 (2013) 5743–5755.
[8] Y. Zhao et al., Scripta Mater. 135 (2017) 54–58.
[9] H. Luo et al., Sci. Rep. 7 (2017) 9892.
[10] K. Ichii et al., Scripta Mater. 150 (2018) 74–77.
[11] H. Luo et al., Corros. Sci. 136 (2018) 403–408.
[12] H.K. Birnbaum, P. Sofronis, Mater. Sci. Eng., A 176 (1994) 191–202.
[13] J. Song, W. Curtin, Nat. Mater. 12 (2013) 145.
[14] R. Kirchheim, Prog. Mater Sci. 32 (1988) 261–325.
[15] R. Kirchheim et al., in: M.F. Ashby, J.P. Hirth (Eds.), Perspectives in Hydrogen in Metals, Pergamon Press, Pergamon, 1986, pp. 95–98.
[16] R.W. Smith, G.S. Was, Phys. Rev. B 40 (1989) 10322–10336.
[17] P. Cotterill, Prog. Mater. Sci. 9 (1961) 205–301.
[18] D. Shih et al., Acta Metall. 36 (1988) 111–124.
[19] D. Xie et al., Nat. Commun. 7 (2016) 13341.
[20] X. Wei et al., RSC Adv. 6 (2016) 27282–27292.
[21] M.S. Daw, M.I. Baskes, Phys. Rev. Lett. 50 (1983) 1285.
[22] T. Michler et al., Corros. Sci. 50 (2008) 3519–3526.
[23] T. Michler, J. Naumann, Int. J. Hydrogen Energy 33 (2008) 2111–2122.
[24] L. Zhang et al., Acta Mater. 56 (2008) 3414–3421.
[25] G. Han et al., Acta Mater. 46 (1998) 4559–4570.
[26] T. Ogata, AIP Conf. Proc. 986 (2008) 124–131.
[27] T. Fang et al., Science 331 (2011) 1587–1590.
[28] W.L. Li et al., Scripta Mater. 59 (2008) 546–549.
[29] N. Stepanov et al., Intermetallics 59 (2015) 8–17.
[30] B. Gludovatz et al., Science 345 (2014) 1153–1158.
[31] M. Dao et al., Acta Mater. 54 (2006) 5421–5432.
[32] R. Schwaiger et al., Acta Mater. 51 (2003) 5159–5172.
[33] S. Bechtle et al., Acta Mater. 57 (2009) 4148–4157.
[34] Z. Zhang et al., Acta Mater. 113 (2016) 272–283.
[35] A. Nagao et al., Acta Mater. 60 (2012) 5182–5189.
[36] M. Nagumo, in: M. Nagumo (Ed.), Fundamentals of Hydrogen Embrittlement, Springer Singapore, Singapore, 2016, pp. 137–165.
[37] S. Wang et al., Acta Mater. 69 (2014) 275–282.
[38] R. Oriani, P. Josephic, Acta Metall. 25 (1977) 979–988.
[39] A. Raina et al., Acta Mater. 144 (2018) 777–785.
[40] T. Watanabe, Mater. Sci. Eng., A 176 (1994) 39–49.
[41] M. Seita et al., Nat. Commun. 6 (2015) 6164.
[42] H. Zhou, H. Gao, J. Appl. Mechanics 82 (2015) 071015.
[43] S.-W. Kim et al., Acta Mater. 60 (2012) 2959–2972.
[44] X. Li et al., MRS Bull. 41 (2016) 298–304.
[45] A. Zaddach et al., JOM 65 (2013) 1780–1789.
[46] P.J. Ferreira et al., in: A.C. Ferro, J.P. Conde, M.A. Fortes (Eds.), Intergranular and Interphase Boundaries in Materials Mater. Sci. Forum, Vol. 207–209, Trans Tech Publications Inc., Switzerland, 1996, pp. 93–96.
[47] J. Hermida, A. Roviglione, Scripta Mater. 39 (1998) 1145–1149.
[48] Q. Liu et al., Corros. Sci. 87 (2014) 239–258.
[49] D. Ulmer, C. Altstetter, J. Mater. Res. 2 (1987) 305–312.
[50] D. Pérez Escobar et al., Corros. Sci. 53 (2011) 3166–3176.
[51] L. Lu et al., Science 304 (2004) 422–426.
[52] L. Zhu et al., Acta Mater. 59 (2011) 5544–5557.